Lab Notes

Editors

Thomas M. Moses | Shane F. McClure
Sally Eaton-Magaña | Artitaya Homkrajae

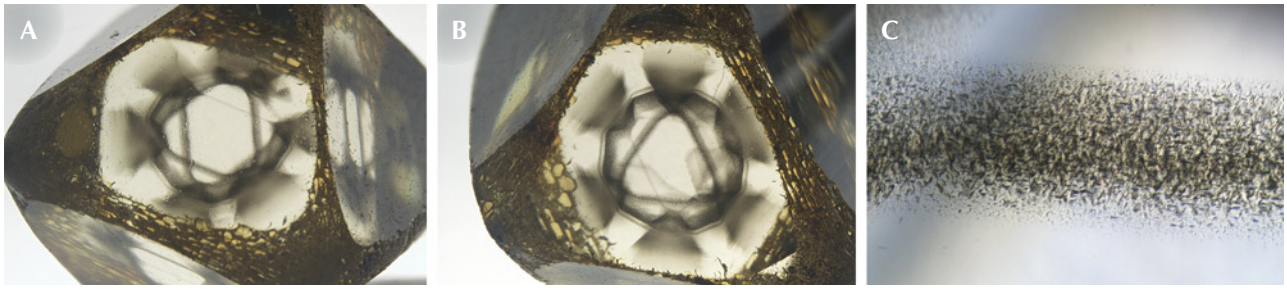

Figure 1. This 3.45 ct natural diamond was partially faceted to highlight the unusual clouds composed of dark micro-inclusions (A and B). At higher magnifications, the distinct micro-inclusions can be observed (C). Photomicrographs by Taryn Linzmeyer; fields of view 7.19 mm (A and B) and 0.72 mm (C).

Unusual Patterns in DIAMONDS Composed of Dark Micro-Inclusions

Recently, at the Carlsbad laboratory, the authors studied two diamonds, submitted separately for scientific examination, with interesting appearances due to the presence of dark micro-inclusions.

The first stone, a 3.45 ct diamond reportedly from Zimbabwe, was partially faceted with rough surfaces preserved along the edges (figure 1A). The stone had six-lobed asteriated inclusion sectors, with a six-sided star pattern visible in the center. When tilted to view through a different facet, some of the star's points were fainter, making the pattern appear as a triangle (figure 1B). These patterns were formed by dark micro-inclusions (figure 1C), concluded as graphite from visual examination.

The visible/near-infrared (Vis-NIR) absorption spectra showed the nitrogen-related features N3 and H3, the radiation-related feature GR1, and a hydrogen-related band at 835 nm. Pronounced brown radiation staining was observed on the unpolished surfaces. The infrared (IR) absorption spectrum confirmed the diamond as type Ia with high amounts of nitrogen and hydrogen, consistent with other diamonds exhibiting similar inclusion scenes (Fall 2019 Lab Notes, p. 417; Fall 2021 *G&G* Micro-World, pp. 269–270; Summer 2024 Lab Notes, pp. 212–214). The inclusion patterns formed in such natural diamonds are often symmetrical and can appear as various configurations of lobed "stars" or triangles when viewed through the polished windows. This diamond was unusual as it showed the graphitic clouds radiating outward starting from the central figure—a pattern not previously seen by the authors.

The second natural diamond was faceted and displayed dark clouds of micro-inclusions with clear openings in the center of the main facets (figure 2). IR absorption spectroscopy indicated that the 13.89 ct stone was also type Ia with hydrogen-related defects. Photoluminescence (PL) mapping using 455 nm laser excitation revealed that the dark cloud inclusion sectors correlated with high concentrations of the S3 defect (figure 3A). This nickel-related peak (A.M. Zaitsev, *Optical Properties of Diamond: A Data Handbook*, Springer-Verlag, Berlin, 2001) caused the clouds to fluoresce green when exposed to long-wave UV, such as in the cloud-inclusion sectors observed in asteriated diamonds (e.g., Fall 2019 Lab Notes, p. 417; Summer 2024 Lab Notes, pp. 212–214). PL spectra within the cloud sector using 532 nm excitation also showed another potentially nickel-related feature at ~694.3 nm.

The stone also contained etch channels passing through clear openings of the clouds. Within the etch chan-

Editors' note: All items were written by staff members of GIA laboratories.

Gems & Gemology, Vol. 61, No. 2, pp. 172–182.

Figure 2. As seen from each main facet, this 13.89 ct natural diamond displays black cloud inclusion sectors with clear openings in the center. Photos by Annie Hayes.

nels, brown radiation stains and a high concentration of PL features were detected, such as NV^- (figure 3, B and C), GR1, and a peak at 588.6 nm. These defects may have been produced by radioactive fluids entering the etch channel while in the earth, creating the resulting stains; subsequent annealing could then create higher concentrations of several vacancy-related centers such as NV^-.

Although both of these diamonds have similar infrared spectra, radiation staining, and the presence of dark microinclusions, the diamonds manifest these characteristics in different ways. They provide another example that all natural diamonds have their own journey and origin story.

Taryn Linzmeyer and Sally Eaton-Magaña

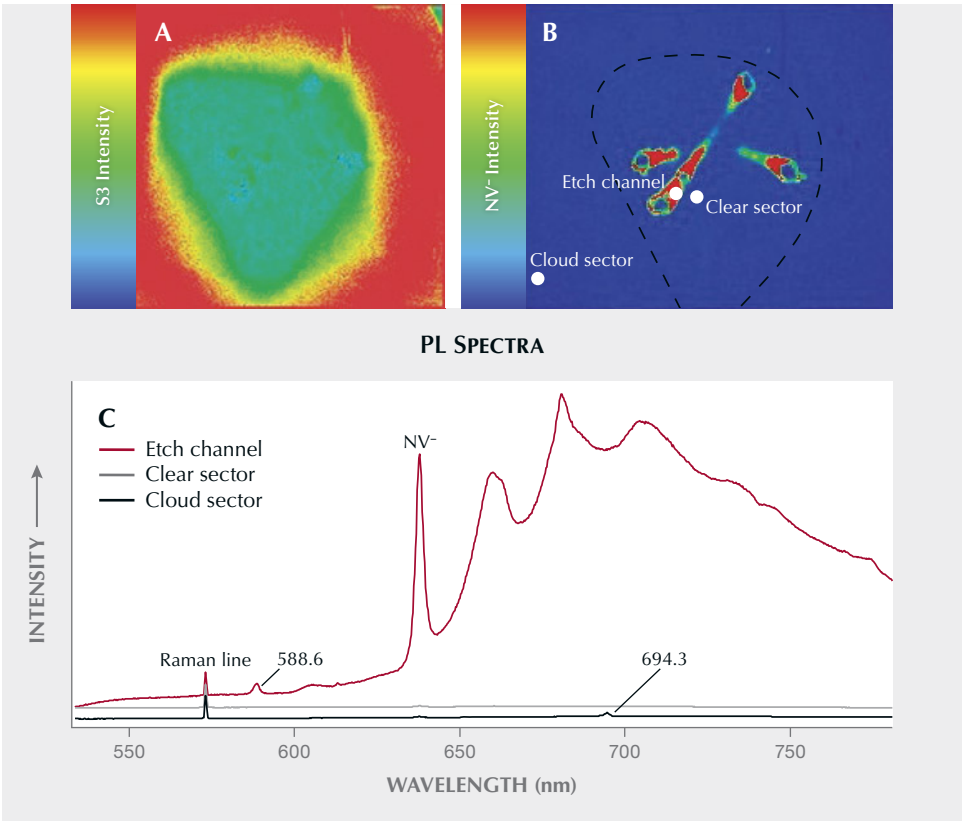

Figure 3. A: False-color 455 nm PL map of one of the 13.89 ct diamond's faces showing a high concentration of the nickel-related S3 center in the dark clouds of micro-inclusions, compared with the clear opening in the center. B: The false-color 532 nm PL map indicates that a high concentration of NV^- defect exists within the etch channels; the dashed line indicates the boundary of the clear opening in the cloud inclusions. Spots of the extracted PL spectra plotted in C are marked with white dots. C: PL spectra collected from the etch channel, clear sector, and cloud sector of the stone are overlaid with Raman lines scaled to equal intensities.

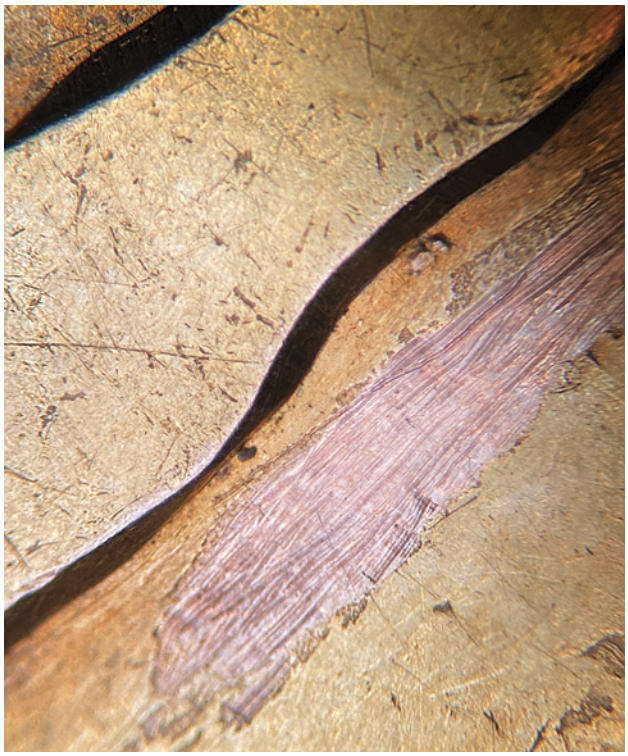

Figure 4. In this gold-plated rose gold item submitted as 14K, the rose gold base tested 9K and the yellow gold layer tested 13.5K. Photo by Carlos Bautista.

Gold-Plated GOLD

GIA's new jewelry verification service examines hundreds of jewelry pieces each day to determine the identity of the metals and mounted gemstones. Recently, the Carlsbad laboratory identified a method that might be used to deceive customers. Adding a layer of gold plating to a gold alloy affects the X-ray fluorescence (XRF) results, and depending on the thickness of the plating, false results can be obtained. XRF metal testing is one of the most reliable ways to analyze metal composition in the jewelry industry, and it can also detect thin plating when the top metal layer differs from the base layer. This method is unreliable, however, when a piece of metal is coated with the same element; therefore, visual observation under a microscope is essential to check for metal discoloration, plating damage, or previous destructive testing that exposes the base material.

We have seen an abundance of gold items plated with gold. This practice is used to change the color of a rose or white gold piece to yellow (figure 4) or to revive the luster in a dull piece of thin yellow gold. Application of plating can be deceitful, as the practice can cause the XRF to determine an inaccurately high gold purity for a piece. For example, coating 10K gold with a precise amount of gold plating can alter the XRF results, identifying the alloy as 14K or 18K gold without detecting any of the plating (figure 5). This is particularly harmful to the consumer if the seller does not disclose this practice and sells alloys with a lower gold content than stated, especially with gold prices reaching all-time highs.

Carlos Bautista

LABORATORY-GROWN DIAMONDS

CVD-Grown Diamond with Unusual Cause of Greenish Color

Recently, the Carlsbad laboratory received a fancy-color diamond grown by chemical vapor deposition (CVD) for a grading report. The 3.07 ct oval brilliant received a color grade of Fancy Light brownish greenish yellow (figure 6)

Figure 5. In this gold-plated pendant submitted as 18K solid gold, the base layer tested 10K and the top layer tested 18K. Arrows show where the gold plating has rubbed off due to use. Photo by Diego Sanchez.

Figure 6. This 3.07 ct HPHT-treated CVD-grown diamond received a color grade of brownish greenish yellow, with the causes of color including isolated nitrogen and SiV^- centers. Photo by Diego Sanchez.

and a clarity grade of VS_1 due to the presence of some graphitic pinpoints. The photoluminescence (PL) spectra and DiamondView fluorescence imaging confirmed a CVD origin and post-growth high-pressure, high-temperature (HPHT) treatment.

The CVD-grown diamond's infrared absorption spectrum showed a weak 1344 cm^{-1} peak with an isolated nitrogen concentration of ~2 ppm. The visible/near-infrared (Vis-NIR) absorption spectrum shows a featureless absorption rise within the blue wavelengths due to the isolated nitrogen (figure 7, left). This is the primary cause of the yellow color. The CVD-grown diamond had been HPHT-treated, which is often used with the intention of removing brownish coloration; nevertheless, the color grade does include a brownish modifier. Although we do not know the color of the CVD diamond before HPHT processing, this treatment can enhance yellow coloration in natural diamonds by increasing the single substitutional nitrogen concentration (D. Fisher and R.A. Spits, "Spectroscopic evidence of GE POL HPHT-treated natural type IIa diamonds," Spring 2000 *G&G*, pp. 42–49). Interestingly, this diamond also contains a greenish modifier which is ascribed as likely due to the absorption of SiV^- centers at 737 nm. This absorption within the red portion of the visible spectrum and flanked by nitrogen-related absorption in the blue region created a transmission window within the green that, while subtle, was sufficient to create a detectable greenish color component. PL mapping using 633 nm excitation (figure 7, right) shows a very strong intensity of SiV^- on the majority of the table facet area.

Previously, green color contributions in CVD-grown diamonds have been due to post-growth irradiation to form the GR1 center with its zero-phonon line at 741.2 nm (e.g., Summer 2018 Lab Notes, pp. 215–216). GIA has examined CVD-grown diamonds colored by much stronger absorption of SiV^- centers, but those samples lacked isolated nitrogen absorption and often resulted in colors from pink to brown (S. Eaton-Magaña et al., "Laboratory-grown diamonds: An update on identification and products evaluated at GIA," Summer 2024 *G&G*, pp. 146–167). An internal GIA database search indicated that this was likely the first submitted CVD-grown diamond in which a green color contribution could be attributed to SiV^- at 737 nm instead of GR1 at 741.2 nm.

Sally Eaton-Magaña

Figure 7. Left: Vis-NIR absorption spectrum collected at liquid nitrogen temperature for the 3.07 ct CVD-grown diamond. Right: False-color PL map of the table facet collected with 633 nm excitation. The peak area of the SiV^- color center at 737 nm is normalized by the unsaturated diamond Raman peak area.

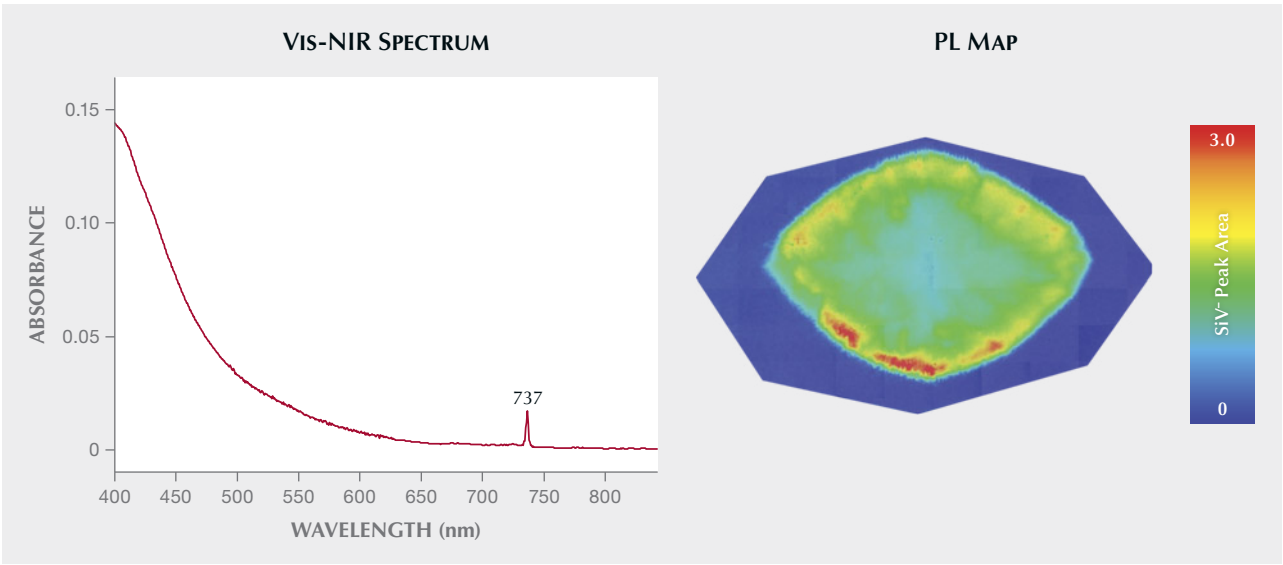

TABLE 1. Comparison of characteristics of submissions with counterfeit inscriptions and their accompanying GIA grading reports.

Samples		Weight (ct)	Measurements (mm)	Color	Clarity	Cut	Polish	Symmetry	Noted inclusions
1	Fraudulent	1.07	6.52–6.56 × 4.04	E	VS1	EX	EX	EX	Feather, internal graining
	Original	1.07	6.51–6.55 × 4.04	E	VVS1	EX	EX	EX	Cloud, pinpoint, feather
2	Fraudulent	1.11	6.63–6.67 × 4.07	E	VVS1	EX	EX	EX	Chip, feather
	Original	1.11	6.61–6.65 × 4.07	E	VVS1	EX	EX	EX	Pinpoint
3	Fraudulent	2.02	8.49–8.53 × 5.09	D	VVS2	EX	EX	VG	Pinpoint
	Original	2.02	8.48–8.54 × 5.10	E	VVS2	EX	EX	EX	Cloud, pinpoint
4	Fraudulent	1.00	6.39–6.45 × 3.93	G	VVS2	VG	VG	EX	Pinpoint, needle
	Original	1.00	6.41–6.46 × 3.92	G	VVS2	EX	EX	EX	Needle, cloud, pinpoint, feather, indented natural, natural

HPHT-Processed Natural and Laboratory-Grown Diamonds with Counterfeit Inscriptions

Recently, the Dubai laboratory encountered four stones submitted for update services inscribed with fraudulent GIA report numbers. Inconsistent font styles and placement indicated the numbers were not authentic GIA inscriptions.

A careful comparison of their quality characteristics confirmed that these were not the same diamonds as described in their accompanying reports. Although the diamonds were carefully selected to closely match the features listed on the original reports, several subtle differences in their color grades, measurements, and other characteristics were identified (table 1). Even more obvious were the spectral differences between the fraudulent and original stones. The difference in the one-phonon region of the Fourier-transform infrared absorption spectroscopy clearly revealed a discrepancy in the diamond types. The diamonds from the original reports were type Ia with aggregated nitrogen impurities, while these submitted stones were all type IIa, confirming they were, in fact, different stones.

On fraudulent diamonds 1 and 2, photoluminescence (PL) spectra produced by 514 nm laser excitation at liquid-nitrogen temperature showed that 637 nm peaks were greater than 575 nm peaks. The 575 and 637 nm peaks are emissions from the nitrogen vacancy center in its neutral $[NV]^0$ and negative $[NV]^-$ charge states, respectively. The 575:637 nm emission ratio of intensities of less than 1 (D. Fisher and R.A. Spits, "Spectroscopic evidence of GE POL HPHT-treated natural type IIa diamonds," Spring 2000 *G&G*, pp. 42–49), along with other PL features, indicated that fraudulent diamonds 1 and 2 with the counterfeit inscriptions were natural diamonds that had undergone high-pressure, high-temperature (HPHT) treatment for color improvements.

The visible/near-infrared (Vis-NIR) absorption spectrum for fraudulent diamond 3, on the other hand, showed a 737 nm peak, which corresponds to the unresolved silicon vacancy $[SiV]^-$ defect at 736.6/736.9 nm commonly seen in laboratory-grown diamonds using the chemical vapor deposition (CVD) growth method (P. Martineau et al., "Identification of synthetic diamond grown using chemical vapor deposition (CVD)," Spring 2004 *G&G*, pp. 2–25). The observation of such features led to the determination that this stone was CVD-grown and subjected to post-grown HPHT processing.

Further PL spectroscopy analysis on fraudulent diamonds 3 and 4 using 633 nm excitation confirmed the presence of the SiV^- doublet feature on both diamonds. In alignment with the Vis-NIR and PL spectra, DiamondView images of these two fraudulent stones displayed clear striations with interruption layers indicative of CVD growth (figure 8). These patterns are consistent with the step-flow growth structure of CVD-grown diamond, which was also visible under the microscope using crossed polarizers and further supported their laboratory-grown origins. The other two fraudulent diamonds (1 and 2), however, showed a lack of such patterns and demonstrated natural-looking features, which confirmed them as HPHT-processed natural diamonds.

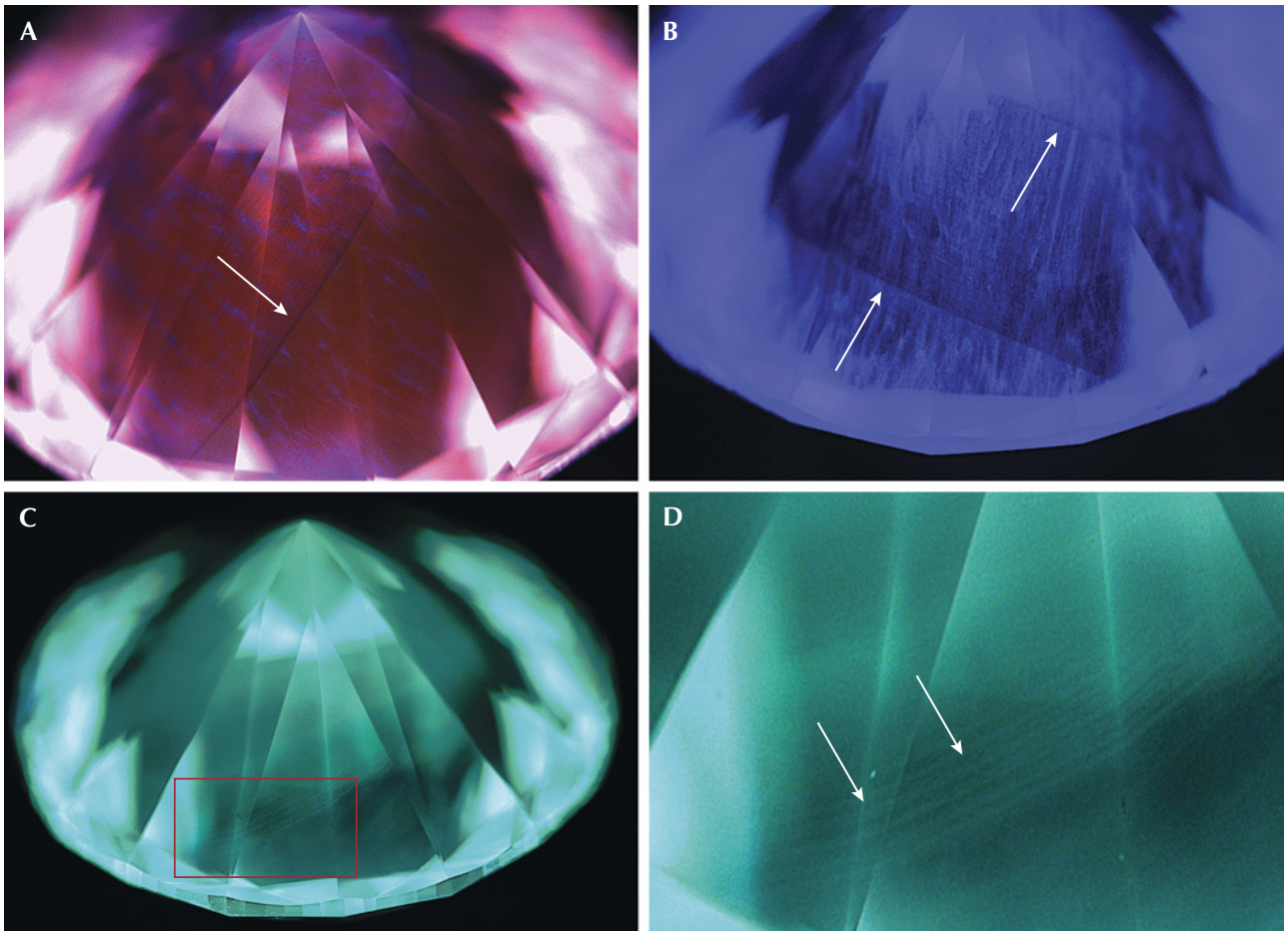

Figure 8. A and B: DiamondView imaging shows clear interruption planes resulting from start-stop environment change during the CVD growth of fraudulent diamond 3. A band pass filter centered at 390 nm shows even clearer interruption layers (indicated by arrows). C and D: Fraudulent diamond 4 shows subtle striations (indicated by arrows) on the pavilion view, but a closer look reveals the layered patterns indicative of CVD-grown diamonds. Images by Nick "Ka Chun" Chan.

Considering all evidence, we concluded that two of the four stones were laboratory-grown diamonds, and the other two were HPHT-processed natural diamonds. All four diamonds were not the same natural diamonds as described in their accompanying GIA grading reports. In accordance with GIA procedures, the counterfeit inscriptions were crossed out (figure 9) and new report numbers were assigned. In addition, GIA inscribes "TREATED COLOR" on natural diamonds with post-treatment history and "LABORATORY-GROWN" along with a GIA report number and distinct GIA LG logo on laboratory-grown diamonds.

Figure 9. GIA's standard procedure is to cross out the counterfeit inscription. Image by GIA staff.

Deceptive practices have occurred previously in the trade; similar instances of diamonds with fraudulent inscriptions have been reported by GIA (e.g., Summer 2021 Lab Notes, pp. 150–152; Fall 2021 Lab Notes, pp. 258–259). Additionally, non-diamond materials, such as synthetic moissanite, with fraudulent GIA inscriptions have been submitted as diamonds to GIA (Fall 2020 Lab Notes, pp. 424–425; Fall 2022 Lab Notes, pp. 360–361). These cases highlight the importance of verifying inscription authenticity because a fraudulent inscription could be overlooked by simple visual examination. One possible solution is GIA's Match iD, a device that compares a diamond's inscription with its grading report in the GIA database.

Nick "Ka Chun" Chan and Satyaprasad Pradhan

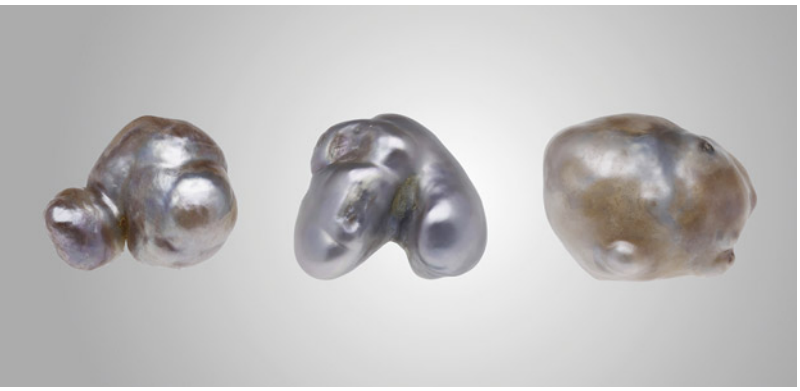

Figure 10. Three large, reportedly natural pearls with hollow interiors from the Pinctada radiata *species from Bahrain, weighing 1.97, 3.92, and 6.13 ct, respectively. Photo by Gaurav Bera.*

PEARLS

Three Large Natural Hollow *Pinctada radiata* Pearls

Recently, three large baroque natural hollow pearls reportedly from the *Pinctada radiata* species were submitted for scientific examination at GIA's Mumbai laboratory. According to the owner, the pearls were obtained from Bahraini divers more than a decade ago. Weighing 1.97, 3.92, and 6.13 ct, and measuring 10.09 × 8.40 × 6.32 mm, 12.78 × 11.12 × 9.45 mm, and 16.00 × 13.94 × 11.60 mm, respectively, these pearls had surprisingly low heft for their sizes (figure 10). Their purplish gray bodycolor, with varying tones of orient, displayed brown patches of different intensities.

Under high magnification, the gray areas exhibited a fine striated nacre growth pattern of overlapping platelets typical of nacreous pearls from *Pinctada* species. Small areas on pearls 1 and 2 displayed a distinctive spiral platy structure, with the translucent outer nacre revealing layers of resinous organic-rich material. In addition, dull brownish patches with a crackled surface texture and a bumpy botryoidal appearance were observed in pearls 1 and 3, surrounded by minor surface blemishes. All three pearls exhibited an inert reaction when subjected to X-ray fluorescence. Energy-dispersive X-ray fluorescence spectrometry showed no traces of manganese and higher strontium levels of 853, 973, and 1013 ppm, respectively, indicative of a saltwater environment. When viewed under long-wave ultraviolet radiation, the pearls showed a moderate bluish green reaction (figure 11) and a similar weaker reaction under short-wave ultraviolet radiation.

Real-time X-ray microradiography (RTX) imaging of all the pearls revealed large voids and organic-rich material of varying opacities extending to the pearls' edges. X-ray computed microtomography (μ-CT) imaging further emphasized the distinct features within these hollow pearls. The large voids consistently followed the outline of

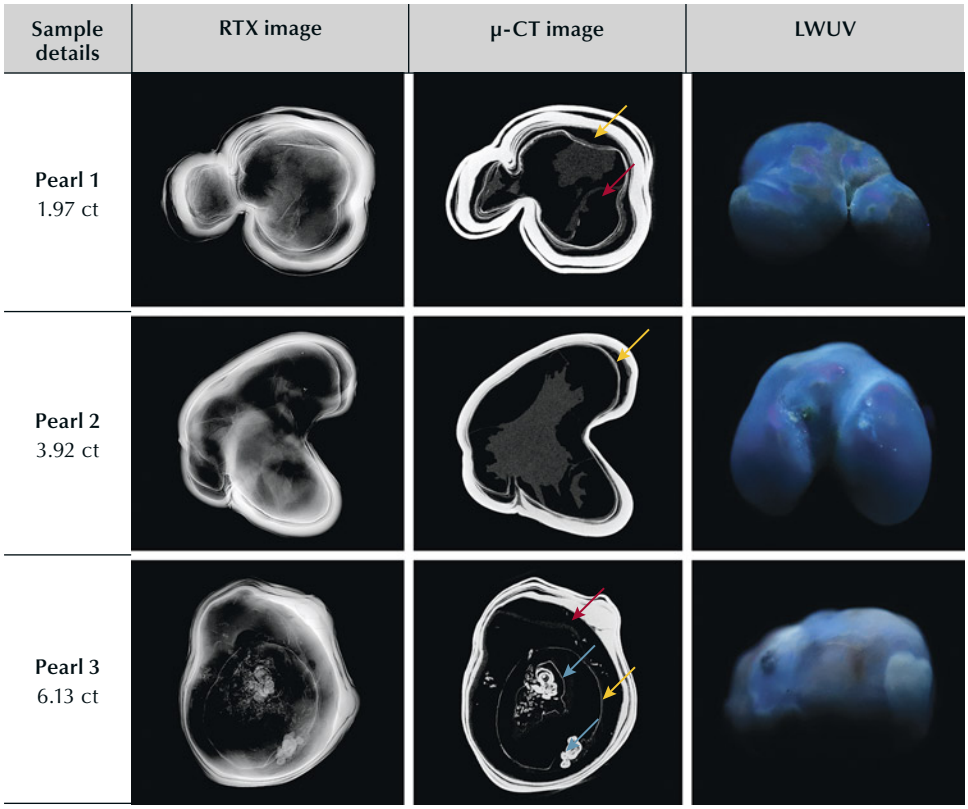

Figure 11. RTX and μ-CT images and long-wave ultraviolet reaction of the three natural hollow pearls. The dark organic-rich voids are marked with red arrows, the white walls are marked with yellow arrows, and the aggregates in pearl 3 are marked with blue arrows. Photos by Gaurav Bera.

Figure 12. The white imitation pearl measuring approximately 1.70 × 1.12 mm and weighing 0.01 ct. Photo by Gaurav Bera.

the pearls and were surrounded by fine growth arcs unlike the typical irregular voids found in non-bead cultured (NBC) pearls, which mostly lack natural growth arcs in the outer nacre ("The microradiographic structures of non-bead cultured pearls," *GIA Research News*, November 20, 2009). In addition, they contained organic-rich material enclosed by white walls that seamlessly followed each pearl's shape. Interestingly, pearl 3 also displayed intriguing concentric aggregates within the void area.

Upon analysis and comparison with reference samples in GIA's research database, it was evident that these specimens closely resembled natural hollow pearls observed in *Pinctada* species. The radiopacity and shape of the voids within them differed from voids typical of saltwater NBC pearls, which tend to be darker, irregular, and more elongated ("Non-bead-cultured pearls from *Pinctada margaritifera*," *GIA Research News*, April 27, 2018). In contrast, the voids in natural hollow pearls exhibit varying degrees of radiopacity. Furthermore, hollow pearls are distinguished by their large, enclosed cavities (*The Pearl Blue Book*, CIBJO, 2023), which sets them apart from solid core pearls.

Notably, many antique pearl jewelry pieces dating before the twentieth century, prior to the start of pearl cultivation, feature large hollow natural pearls. These hollow natural pearls were often too fragile to set on jewelry and were frequently filled with metal fragments to increase both their durability and weight. Despite their significant size, hollow pearls are deceptively light. It is quite common for natural pearls to exhibit a hollow structure. The exploration of such pearls has consistently captivated gemologists, as their intricate and complex internal structures pose challenges in drawing definitive conclusions, with similar voids occasionally observed in NBC pearls. The study of such specimens provides valuable insights and significantly contributes to our understanding of the formation processes associated with natural hollow pearls.

Prasad Mane, Roxane Bhot Jain, and Abeer Al-Alawi

Imitation Seed Pearl with Blue X-Ray Fluorescence

GIA's Mumbai laboratory recently received a submission of 18 strands of pearls for identification, consisting of approximately 9,360 white to light cream pearls weighing a total of 706.79 carats. When subjected to X-ray fluorescence, most of the pearls were inert, indicating a saltwater origin, while a few exhibited the strong yellowish green fluorescence of freshwater pearls. Notably, one white oval "pearl," measuring approximately 1.70 × 1.12 mm and weighing 0.01 ct (figure 12), displayed a unique moderate blue reaction upon X-ray exposure (figure 13)—an effect not previously observed in saltwater or freshwater pearls. The "pearl" was visually similar to the other submitted pearls, but its extremely large drill

Figure 13. Left: The imitation pearl (marked with arrow) in the strand appearing similar to other pearls. Right: When exposed to X-ray fluorescence, it exhibits a blue reaction, while the remaining pearls are inert. Images by Karan Rajguru.

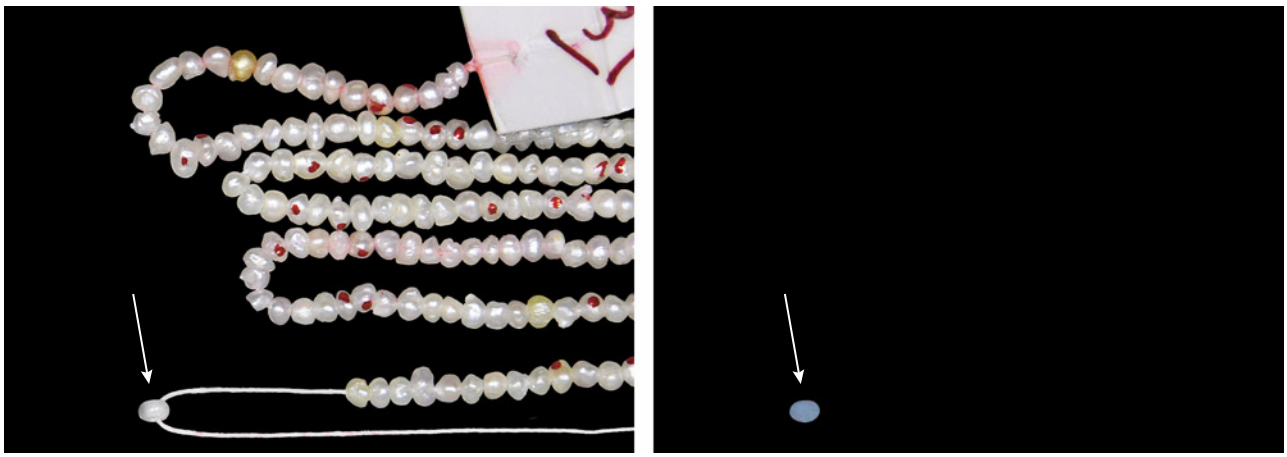

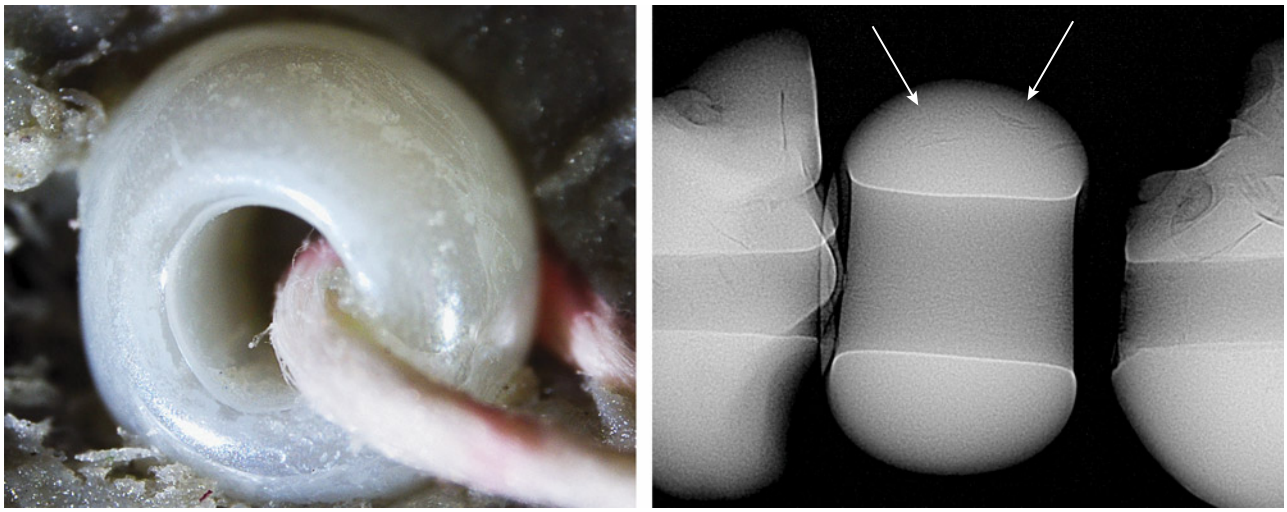

Figure 14. Left: Extremely large drill hole and surface showing liquid-like remnants; field of view 1.6 mm. Right: RTX image revealing arcs in the imitation pearl (indicated by arrows) similar to those of two adjacent natural pearls. Images by Karan Rajguru.

hole raised suspicion (figure 14, left). Under higher magnification, its smooth surface lacked characteristic nacreous overlapping aragonite platelets, displaying a unique liquid-like surface residue instead. This "pearl" appeared inert under long-wave ultraviolet light, while other pearls were greenish yellow. Additionally, it exhibited a light yellow reaction under the deep-UV wavelength (<225 nm) of the DiamondView, unlike the typical blue reactions observed in pearls. Raman spectroscopy with different laser excitations did not reveal any distinctive features indicative of calcium carbonate polymorphs typically found in pearls. Based on these findings, it was concluded that the material in question was not a pearl but rather an imitation. Real-time X-ray microradiography (RTX) indicated that, with the exception of the one imitation, the 18 strands contained a mixture of natural and non-bead cultured pearls. Interestingly, the imitation displayed a similar radiopacity to the other pearls. A few arcs were present at the outer edges, comparable to growth arcs observed in the adjacent natural pearls strung in the strand (figure 14, right).

Common pearl imitations often utilize material such as solid or hollow glass, plastic, or shell bead coated with a "pearl essence" substance that simulates nacre's iridescence (J. Hanano et al., "Majorica imitation pearls," Fall 1990 *G&G*, pp. 178–188). These imitations lack the usual nacreous platelets, mosaic patterns, and cellular structures observed in pearls, and often present a glittery surface appearance of coating material and occasional "molded" drill holes. Such imitations may show variations in RTX results depending on the composition of the substance and the coating.

Distinguishing imitations when mixed with large quantities of pearls in an item can be a challenge. Due to their similarity in appearance, these materials are occasionally mixed with pearl strands and jewelry. Furthermore, the presence of arcs in the examined imitation sample may have been misleading, potentially going unnoticed without the aid of the blue fluorescence under X-ray exposure during routine testing. The utilization of X-ray fluorescence screening has proven useful in the identification of certain types of imitation materials, particularly in the case of smaller pearls strung in strands. While encountering such imitation materials is not frequent in routine testing, it remains essential to accurately distinguish and identify them to maintain the authenticity of pearl collections.

Karan Rajguru, Anukul Belanke, and Abeer Al-Alawi

PEZZOTTAITE with Multiple Cat's-Eyes

An 11.23 ct purplish pink cabochon exhibiting multiple cat's-eye phenomena was recently submitted to the Tokyo laboratory for identification (figure 15, left). Standard gemological testing results included a spot refractive index of 1.59, a specific gravity of 3.11, dichroism, and an inert reaction under both long-wave (365 nm) and short-wave (254 nm) UV radiation. Microscopic observation revealed several inclusions: iridescent parallel growth tubes or elongated thin films, trichite-like iridescent fingerprints, and transparent colorless crystals. The Raman spectrum was consistent with pezzottaite ($CsLiBe_2Al_2Si_6O_{18}$).

Pezzottaite was discovered in Madagascar in 2002 and approved as a new mineral by the International Mineralogical Association in 2004. While it belongs to the beryl mineral group, pezzottaite has a trigonal crystal system, differing from beryl's hexagonal crystal system, and can be described as having imperfect cleavage parallel to the basal {001} planes, which are perpendicular to the *c*-axis (i.e., the optical axis; F.C. Hawthone et al., "Pezzottaite $Cs(Be_2Li)Al_2Si_6O_{18}$: A spectacular new beryl-group mineral

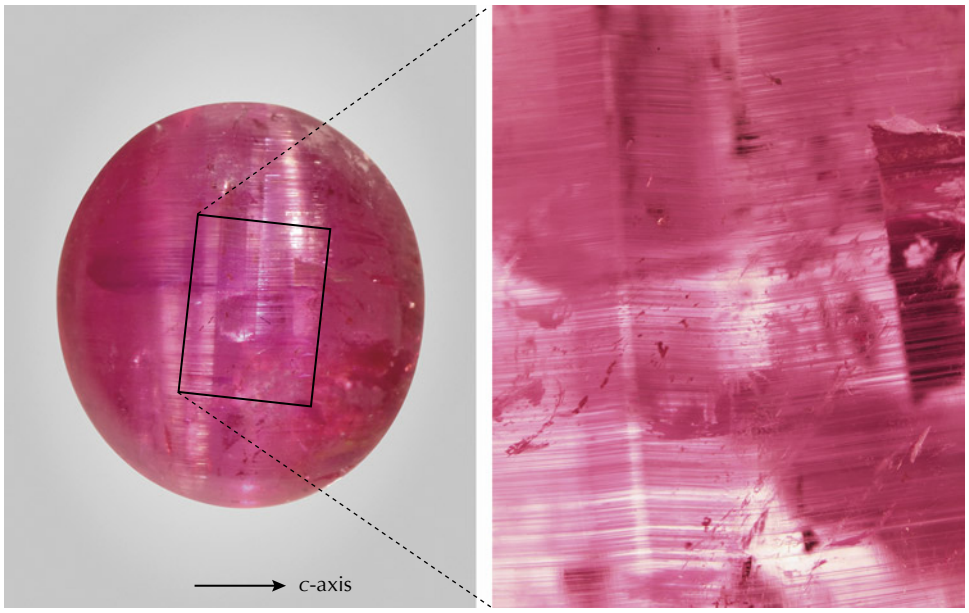

Figure 15. Left: An 11.23 ct purplish pink pezzottaite cabochon, measuring 14.43 × 13.10 × 7.39 mm, displaying multiple cat's-eyes. The arrow indicates the c*-axis (i.e., the optical axis). Photo by Shunsuke Nagai. Right: These cat's-eyes are produced by growth tubes likely bent by imperfect {001} cleavage planes. Photomicrograph by Taku Okada; field of view 4.80 mm.*

from the Sakavalana pegmatite, Fianarantsoa province, Madagascar," *Mineralogical Record*, Vol. 35, No. 5, 2004, pp. 369–378).

In the submitted stone, the growth tubes or elongated thin films were oriented nearly parallel to the *c*-axis and displayed multiple bends possibly resulting from imperfect {001} cleavage planes, producing multiple cat's-eyes perpendicular to them, or almost perpendicular to the *c*-axis (figure 15, right). Though it is unknown how the bending of these inclusions happened, they work together to produce the highly exceptional and impressive phenomenon of multiple cat's-eyes.

Taku Okada and Kazuko Saruwatari

QUARTZ Assemblage Imitating Emerald

Gemstone assemblages, composed of two or more materials fused or bonded together, have long been used to imitate a variety of natural gemstones. These composite constructs are regularly encountered in gemological laboratories, where they are identified by their component parts and may be referred to as imitations of various natural stones. Assembled stones designed to mimic emeralds have historically been constructed using colorless spinel with colored cement, layered glass, or beryl doublets/triplets. One of the most widely encountered assembled emerald imitations is the *soudé emerald*, which entered mass production in the early twentieth century. Over time, its construction evolved from the use of rock crystal to colorless synthetic spinel, and later to colorless beryl or pale aquamarine.

GIA's New York laboratory recently examined a green stone mounted in a necklace with a total weight of 7.84 grams (figure 16). While the deep green color of this stone suggested it may be an emerald, a spot refractive index measurement yielded a value of 1.54, indicating the stone was likely quartz. Under both long- and short-wave ultraviolet radiation, the assemblage exhibited a whitish fluorescence, which was confined to an internal layer within the stone. Raman spectroscopy using a 514 nm laser further confirmed the identification of the material as quartz.

Initial microscopic examination of the green stone revealed a separation plane near the carved top, along with

Figure 16. A pendant necklace featuring a green stone measuring 13.35 × 12.20 × 12.20 mm that was identified as a quartz assemblage. Photo by Michele Wong.

Figure 17. The assemblage appears as two carved pieces attached to the setting with a green cement. Colorless gas bubbles can be observed, an indication that this piece is not what it seems. Photomicrograph by Ezgi Kiyak; field of view 21.2 mm.

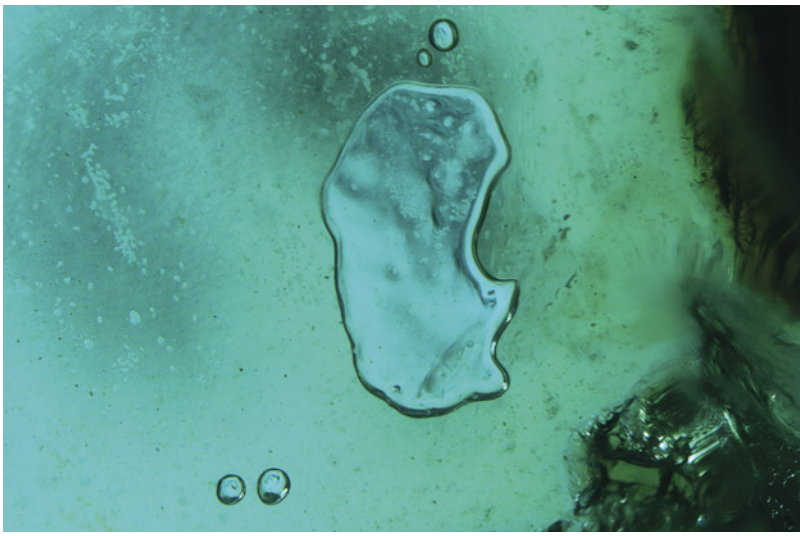

Figure 18. Tabular bubbles in the bluish green cement demarcate the boundary between the quartz segments. Photomicrograph by Hannah Wiggins; field of view 7.19 mm.

numerous gas bubbles, and some large air-filled voids that blocked the cement, creating colorless zones (figure 17). These colorless voids reinforced the observation that the green color appeared to be confined to the cement layer (figure 18). Further inspection under the microscope revealed natural fluid inclusions, supporting the identification of natural rock crystal quartz.

This detailed examination of the green stone exposed three sections of colorless natural quartz in various thicknesses joined with a green-colored cement, prompting the authors to collect X-ray tomography images to investigate how the green stone was assembled. The X-ray computed tomography showed three distinct quartz components connected by a cement layer with an average thickness of 0.20 mm along a clearly defined interface (figure 19). The exceptionally precise machining of the parts of this assemblage makes this piece a particularly sophisticated assembled stone.

Hannah Wiggins and Ezgi Kiyak

Figure 19. A and B: 3D scanned images indicating the colored cement layer between the carved parts. C: The carving details from the outside. Images by Emiko Yazawa and W. Henry Towbin.